

QoE Driven VR 360° Video Massive MIMO Transmission

Long Teng, Guangtao Zhai, *Senior Member, IEEE*, Yongpeng Wu, *Senior Member, IEEE*, Xiongkuo Min, *Member, IEEE*, Wenjun Zhang, *Fellow, IEEE*, Zhi Ding, *Fellow, IEEE*, and Chengshan Xiao, *Fellow, IEEE*

Abstract

Massive multiple-input and multiple-output (MIMO) enables ultra-high throughput and low latency for tile-based adaptive virtual reality (VR) 360° video transmission in wireless network. In this paper, we consider a massive MIMO system where multiple users in a single-cell theater watch an identical VR 360° video. Based on tile prediction, base station (BS) delivers the tiles in predicted field of view (FoV) to users. By introducing practical supplementary transmission for missing tiles and unacceptable VR sickness, we propose the first stable transmission scheme for VR video. We formulate an integer non-linear programming (INLP) problem to maximize users' average quality of experience (QoE) score. Moreover, we derive the achievable spectral efficiency (SE) expression of predictive tile groups and the approximately achievable SE expression of missing tile groups, respectively. Analytically, the overall throughput is related to the number of tile groups and the length of pilot sequences. By exploiting the relationship between the structure of viewport tiles and SE expression, we propose a multi-lattice multi-stream grouping method aimed at improving the overall throughput for VR video transmission. Moreover, we analyze the relationship between QoE objective and number of predictive tile. We transform the original INLP problem into an integer linear programming problem by setting the predictive tiles groups as some constants. With variable relaxation and recovery, we obtain the optimal average QoE. Extensive simulation results validate that the proposed algorithm effectively improves QoE.

Index Terms

L. Teng, G. Zhai, Y. Wu, X. Min, and W. Zhang are with the Institute of Image Communication and Information Processing, Shanghai Jiao Tong University, Shanghai 200240, China (e-mail: tenglong@sjtu.edu.cn; zhaiguangtao@sjtu.edu.cn; yongpeng.wu@sjtu.edu.cn; minxiongkuo@sjtu.edu.cn; zhangwenjun@sjtu.edu.cn). (*Corresponding authors: G. Zhai and Y. Wu.*)

Z. Ding is with the Department of Electrical and Computer Engineering, University of California at Davis, Davis, CA 95616 USA (e-mail: zding@ucdavis.edu).

C. Xiao is with the Department of Electrical and Computer Engineering, Lehigh University, Bethlehem, PA 18015 USA (e-mail: xiaoc@lehigh.edu).

Tile-based adaptive VR 360° video, field of view (FoV), tolerant latency, tile grouping, massive MIMO, quality of experience (QoE), linear programming

I. INTRODUCTION

The recent explosive growth of smart devices and multimedia services strongly motivate the development of new technology to deliver virtual reality (VR) 360° video across wireless networks. The ultra-high resolution, high representation, panoramic scene, and multi-stimuli of VR provide a unique immersive experience, allowing users to interact within an alternative world. Unlike traditional video, panoramic scene of VR 360° video is captured by omnidirectional cameras. While watching VR videos, users may freely adjust orientation to retrieve expected immersive scene as part of VR user interaction with support from interactive sensors [1].

As discussed in [2], transmitting VR 360° video, characterized by ultra-high data rate and low latency, presents critical challenges to wireless networking. Recent works have focused on compressing the required data payload in the area of VR 360° video processing. For example, VR 360° video is projected into a specific 2-D plane with multiple slices, and encoded with a established rule [3]. Generally, delivering all slices is unnecessary considering that the field of view (FoV) is limited. Transmitting only desired slices is able to decrease the data size to effectively relieve network load [4]. Despite such efforts, transmitting ultra-high resolution VR video in real-time remains unrealistic under limited wireless bandwidth and throughput. Long transmission latency can cause human VR sickness. An alternative proposal is to apply content buffering or caching [5], [6] in wireless edge or device in advance. To this end, content prediction is necessary. Buffering predicted contents in devices before playback and adjusting the sequence of encoded segments to reduce response latency are likely to lessen the impact of random head movement [7] and the VR sickness caused by stall [2].

Content prediction techniques in VR mainly include saliency prediction and quality assessment. Saliency [8] can describe the importance of different visual contents and can be used to obtain the scope of the most visually appealing areas automatically. Quality assessment has also been widely used to analyze VR 360° video content. For example, [9] proposes a blind image quality assessment model based on multi-channel convolutional neural network (CNN) architectures to accumulate the objective quality scores of the VR 360° video, which can help derive the probable slices of interest. The success of CNN in slice prediction for VR 360° image [10] and VR 360° video [4], [11] confirms the capability of learning based approach according to the user behaviors in predicting the “exact scope”. In fact, we leverage the result of exact scope in next model and formulation. In particular, [12] utilizes gaze-aware streaming to limit the provisioning of high video quality to areas near users’ fixations, without quality loss in user perception.

Omnidirectional video coding is also an important element in VR. High efficiency video coding (HEVC) [13] is standardized collaboratively by a joint video exploration team (JVET) of ITU-T VCEG and ISO/IEC MPEG organizations, and the joint exploration model beyond HEVC developed by JVET provides a well-performing encoder with manageable complexity, with potential to improve the coding efficiency significantly. In terms of sphere-to-plane coding on head mounted display (HMD), the work in [14] shows that equirectangular format saves 8.3% bit rate traffic. Considering the equirectangular format of VR 360° video, tile-based projection (TBP) [11], [15]–[17], which splits the high resolution video into several tiles, effectively reduces the transmitted data with low distortion according to the viewport of user [3]. TBP is widely used in the projection process of VR video and exhibits strong advantages in multicast application [18]¹. Hence, in this work we apply the TBP with reasonable tile size to transmit VR 360° video in wireless network.

Most existing VR 360° video transmission schemes explore the optimization algorithms in a certain wireless network. With optimal transmission time and power allocation, [20] searches the multicast opportunity to respectively minimize the average transmission energy for the given video quality and maximize the video quality for the given energy budget in a time division multiple access (TDMA) system. Based on the concept in [20], work in [21] exploits user transcoding and transcode-playback mode aimed to maximize the multicast opportunity with the consideration of smoothness requirement in a TDMA system. [22] defines a performance metric for perfect, imperfect and unknown FoV probability distributions, and maximize the performance metric in a multi-carrier system.

In VR video transmission, the quality of experience (QoE) is paramount. Factors restricting QoE of VR video have been extensively investigated in [7], [17], [23]–[26]. Most previous works adopt mean opinion score based on subjective quality evaluation. Summarizing the works of [7], [17], [23]–[26], there are three major factors of VR quality that should be investigated in wireless applications. The first is the overall tile quality perceived by multiple users, which relates to the network capacity. The second is the uncomfortable visual perception caused by quality differences among tiles. The third is the stall time caused by low transmission rate or data retransmission. Thus, we consider these three major factors in the QoE model. Note that the stall time longer than tolerant latency is a major cause for VR sickness.

To the best of our knowledge, the performance of existing wireless transmission methods of VR 360° video has been less than satisfactory. The major obstacle is the poor tile quality caused by the low link throughput. Moreover, current works focusing on VR video transmission in wireless networks [11], [18], [23], [27] generally assume that the exact FoV can be predicted infallibly from machine learning and only

¹Compared with unicast, multicast can substantially improve the overall achievable throughput [19].

transmit the predicted FoV. In addition, existing works, e.g., [20]–[22] try to search the exact FoV through the viewing probability distribution, which leads to inaccurate results or requires many more tiles for transmission. In practice, for the reason of exceptional head movement caused by multi-stimuli [24], e.g., when user is watching a scene with multi-stimuli like racing and roller coaster, the FoV is difficult to be predicted reliably and a much larger scope of tiles must be considered. In short, existing VR transmission works have not systematically considered the real supplementary transmission for missing tiles, which is likely to cause unacceptable latency, and perceptual difference due to spatial quality variance. These shortcomings present challenges to user QoE of VR delivered over wireless network.

Massive multiple-input and multiple-output (MIMO) [28], can overcome effects of uncorrelated noise and fast fading and deliver multiple streams to their respective users simultaneously. Base stations (BSs) equipped with large-scale antenna arrays can effectively exploit the estimated channel matrix [29] to provide high sum-rate [30] and signal quality [31]. Thus, massive MIMO has the potential to wirelessly achieve the VR need for high-throughput and low access latency [32]. Moreover, the multiple tiles, treated as multiple streams, can be easily transmitted to users simultaneously by taking advantage of the massive MIMO systems. Integrating massive MIMO within VR video transmission has strong potential to improve the QoE. Surprisingly, there has been very few existing efforts in this direction.

Existing works in [20]–[22] have proven that grouping and multicast can efficiently improve network throughput. However, the multicast [20]–[22] is uni-stream multicast in TDMA. Moreover, there has been no prior work that systematically combines the multi-stream multicast massive MIMO and VR 360° video transmission in the QoE optimization. Motivated by the need for supplementary transmission for missing tiles and the potential offered by massive MIMO, we consider a practical and innovative scenario involving QoE driven transmission of VR 360° video in multi-user massive MIMO wireless networks. In this multicast setting, multiple users in a single-cell massive MIMO systems are engaged in the same VR 360° video. Our goal is to implement the tile grouping and determine the quantity of predictive tiles for maximizing the average QoE. Specifically, the main contributions of this paper are summarized as follows:

- We investigate the QoE driven VR 360° video transmission in multi-user massive MIMO systems, and systematically combine multi-stream multicast massive MIMO and VR 360° video transmission in the QoE optimization. According to the real supplementary transmission for missing tiles and the unacceptable VR sickness, we propose a practical and stable transmission scheme. We formulate the average QoE objective of watching an identical VR 360° video.
- We derive a closed-form expression of the achievable spectral efficiency (SE) of predictive tile groups and the approximately achievable SE of missing tile groups under the maximum ratio

transmission (MRT) and zero-forcing (ZF) precoding schemes, and allocate precoding power to guarantee consistent delivery rate of each stream based on max-min fairness (MMF).

- We analyze the relationship between SE and viewport tiles, and prove the existence of an optimal multi-stream grouping based on rectangular viewport. We further propose a multi-lattice multi-stream grouping (MLMSG) method to reduce the transmitted groups and pilot sequences during multicast.
- We adopt a variable number of predictive tiles. By setting the number of predictive tile groups as some constants, the original integer non-linear programming (INLP) problem is transformed into an integer linear programming (ILP) problem to optimize the final average QoE through relaxation and recovery. Extensive simulations demonstrate that the proposed algorithm effectively improves VR 360° video QoE at low complexity.

The remainder of this paper is organized as follows. We present the system model and problem formulation in Section II. Section III derives the achievable SE of each group tile in massive MIMO system. And we propose the MLMSG in Section IV. In Section V, we maximize the average QoE by turning the non-linear problem into a linear problem. Simulation results are presented in Section VI to evaluate the performance of our proposed algorithm. We finally conclude our paper in Section VII.

Notations: Lower case, boldface lower case, and boldface upper case letters denote scalars, vectors, and matrices, respectively; \mathbf{I}_N denotes the identity matrix of size N . $\mathbf{x} \sim \mathcal{CN}(\mathbf{0}, \Sigma)$ indicates that \mathbf{x} is a circularly symmetric complex Gaussian vector with zero mean and covariance matrix Σ . The superscripts $(\cdot)^T$, $(\cdot)^*$, and $(\cdot)^H$ stand for the transpose, conjugate, and conjugate-transpose of a matrix, respectively. We use $\mathbb{E}\{\cdot\}$ to denote ensemble expectation and $|\mathbf{x}|$ to represent cardinality of a set \mathbf{x} . $\lceil x \rceil$ and $\lfloor x \rfloor$ stand for the smallest integer larger than or equals to x and the largest integer smaller than or equals to x , respectively.

II. SYSTEM MODEL AND PROBLEM FORMULATION

In this section, we introduce the system model which contains the tile-based adaptive regime in VR video processing and the considered deployment scenario in wireless network. Then the problem formulation maximizing the average QoE is presented.

A. Tile-Based Adaptive Regime

VR 360° video captured and stitched by omnidirectional camera has a spherical shape in the original format. For a watching user, the scene within viewport is displayed in the HMD, and user can turn their head and eyes to track the interesting contents as illustrated in Fig. 1(a). Utilizing the typical tilling approach [3], the whole spherical streaming is projected into an equirectangular format with multiple

sized tiles as shown in Fig. 1(b), which can be encoded according to a set of quality levels. It is noted that the equator of VR sphere is projected into the horizontally intermediate line of equirectangular. Denote the coordinate origin as O , the horizontal coordinate set as \mathcal{H} , and the vertical coordinate set as \mathcal{V} , then the tile index in the equirectangular can be represented by $\zeta(x, y), x \in \mathcal{H}, y \in \mathcal{V}$. Without moving head, FoV covering 150° horizontally and 120° vertically including eyes movement is recommended in [2]. Accordingly, the tiles contained FoV are encoded in high quality and the remaining ones can be encoded in basic low-quality or abandoned to improve the QoE under limited network capacity. Simultaneously, HMD sensors can feel user movement and activities, and can provide helpful information to predict the desired tiles and implement tile-based adaption.

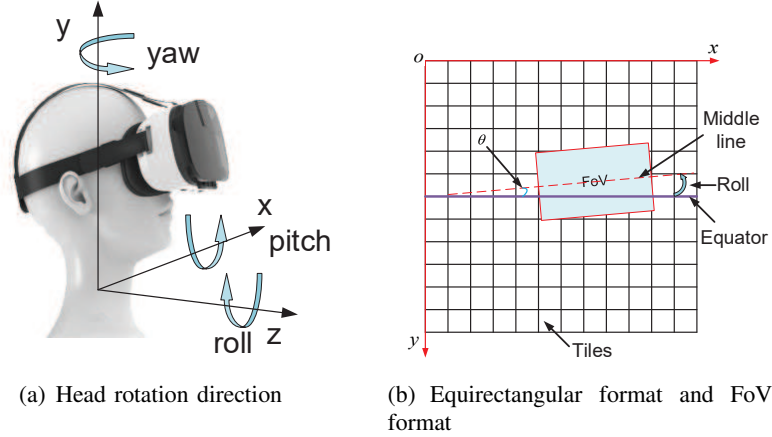


Fig. 1. (a) Head rotation model; and (b) equirectangular projection based on tiling approach.

B. Deployment Scenario

We consider an open VR theater with seats arranged in multiple cycles in a single-cell, where each user wears a single-antenna HMD and seats on a rotatable but fixed chair. There are K active users indexed by set $\mathcal{K} = \{1, \dots, K\}$ and the transmission bandwidth is W . The scenario is illustrated in Fig. 2, where the BS equipped with N antennas locates in the center to serve the K active users simultaneously in the time division duplexing (TDD) mode. The powers of HMD and BS are denoted as P_u and P_d , respectively. In the scenario, the radii of inner cycle and outer cycle are r_1 and r_2 , respectively.

Assume a block-fading channel model which remains invariant in each coherence interval T , where T is the product of the coherence bandwidth C_B and coherence time C_T . Further, the duration of exceptional head movement is relative small compared with the coherence time such that Doppler frequency offsets can be negligible. In the system, we consider uncorrelated Rayleigh fading channel

responses, and denote \mathbf{h}_k as the channel response of user k , i.e., $\mathbf{h}_k \sim \mathcal{CN}(\mathbf{0}, \psi_k \mathbf{I}_N)$, where ψ_k is the large-scale fading coefficient. Note that practical channels might have spatially correlated fading or line of sight components, but theoretical studies and practical measurements carried out in real massive MIMO propagation environments have shown that SE can be predicted using uncorrelated fading models [33]. Moreover, this channel model enables us to present novel insights into VR 360° video massive MIMO transmission.

Within each coherence interval, we focus on uplink pilot transmission and downlink data transmission. During uplink pilot transmission, users send uplink pilots to enable BS to estimate their respective uplink channels. The pilots in classic unicast massive MIMO system are orthogonal. Applying the concept of co-pilot proposed in [19], the users assigned to receive the same tile would share a pilot in each multicast stream. It is therefore reasonable to assume that the pilots of different streams are orthogonal. Taking advantage of reciprocity between uplink and downlink channels in TDD, the BS performs downlink precoding based on the estimated channels and delivers the tile.

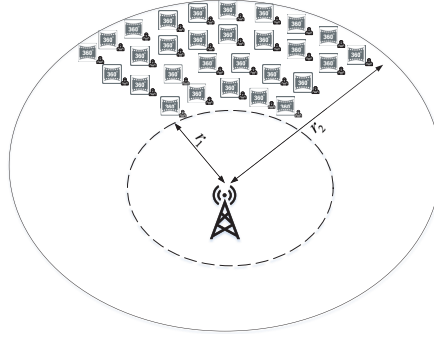


Fig. 2. Multiple users experiencing VR 360° video in a massive MIMO cell.

The FoV can move arbitrarily by rotation in the directions of pitch, yaw, and roll. Denote the angle between the middle line of viewport and equator as θ , which is influenced by the rotation in the direction of roll. We illustrate the relationship between θ and roll direction in Fig. 1(b). It was shown in [34] that a large proportion of fixation distributes near the equator, and the authors of [11] stated that rotation in the direction of roll is negligible compared with the other two directions. Hence, we mainly focus on $\theta = 0$ where predictive FoV tiles are rectangle in shape. Further, the number of tiles different between the FoV and the exact scope is directly and positively correlated to the distribution area of multi-stimuli around a certain viewport [4]. Over 80% prediction accuracy can be obtained by machining learning [4], [35]. Thus the exact scope that can be predicted is consequently a little larger than the FoV. In addition, the structural similarity proposed in [36] recommends that the predictive tiles reside in the middle of the

exact scope. We apply this concept in tile buffering. For clarity, we illustrate the case in Fig. 3. Without fully accurate prediction, BS transmits desired missing tiles, i.e., the tiles within exact scope outside the predictive set, to supplementally meet user needs. The BS has completely cached the original VR 360° video and the HMD has ability of buffering and computing. The BS leverages the existing CNN prediction model to calculate the prospective viewports of each user, and transmits the corresponding data to HMDs in advance. Having received the transmitted data, the HMD selectively arranges the tiles, stitches 2-dimensional (2D) tiles into 3-dimensional (3D) FoV, renders and displays the expected scenes.

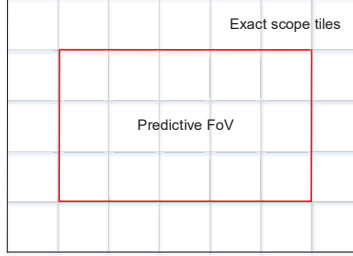


Fig. 3. Representations of predictive FoV and exact scope.

Like traditional video, VR 360° video has similar frame structure and frame size. Based on characteristics of tile prediction, time interval of predictive tiles² should be scheduled reasonably to avoid non-real-time transmission or excessive overhead on computing time and energy. Further, time interval of missing tiles should be short to reduce the stall time. In this work we set T_1 and T_2 as the time intervals of predictive tiles and missing tiles, respectively. All tiles in each interval time include three parts, i.e., the predictive tiles within T_1 , denoted as Z_0 , the missing tiles within T_2 , denoted as Z_1 , and the subsequent missing tiles within $T_1 - T_2$, denoted as Z_2 . Note the transmission order: Z_0 , Z_1 , and Z_2 . Without being content specific, quality level of each tile strictly relates to the set of encoding rates. We denote the encoding rates of predictive tile and missing tile as η_p , and η_m , respectively, which belong to encoding rate set $\mathcal{R} = \{R_1, \dots, R_d, \dots, R_D\}$. For public VR theater, VR sickness due to stalling is unacceptable. Thus, there is an upper bound of tolerable stall time T_y . In addition, assuming user fairness, we make the following assumptions.

Assumption 1:

- 1) The encoding rates of predictive tiles and missing tiles for every user are the same;

²Note that the time interval of predictive tiles is also the corresponding playback time.

- 2) The numbers of predictively transmitted tiles of each frame are the same for each user, denoted as $N_p^k = N_p, \forall k \in \mathcal{K}$; thus the expected numbers of missing tiles of each frame are also the same for each user, denoted by $N_m^k = N_m, \forall k \in \mathcal{K}$.

C. Problem Formulation

In this paper, we maximize the average QoE of VR 360° video transmission in massive MIMO systems by joint consideration among N_p , N_m , η_p , and η_m .

Denote functions $\chi(N_p, Z_0)$, $\chi(N_m, Z_1)$, and $\chi(N_m, Z_2)$ as the transmission latencies of transmitting Z_0 , Z_1 , and Z_2 , respectively, where the size of Z_0 , Z_1 , and Z_2 are $T_1\eta_p$, $T_2\eta_m$, and $(T_1 - T_2)\eta_m$, respectively. To avoid VR sickness caused by stall,

$$\chi(N_m, Z_1) \leq T_y. \quad (1)$$

In addition, during the current playback time T_1 , the transmission of last Z_2 will occupy the current transmission time for current Z_0 . For clarity, we illustrate the scheme in Fig. 4. The first Z_2 and the

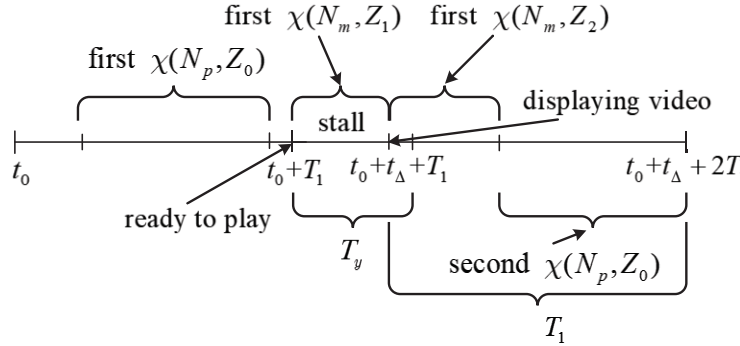


Fig. 4. Stable transmission scheme for Z_0 , Z_1 , and Z_2 .

second Z_0 should be delivered within T_1 , to maintain transmission model stability. Under the identical prediction model and smooth short interval T_1 , the number of missing tiles between two adjacent time intervals are approximately the same. For this reason, we can reasonably assume that Z_0 and Z_2 in the same interval time should be delivered within T_1 . In other words, we require

$$\chi(N_p, Z_0) + \chi(N_m, Z_2) \leq T_1. \quad (2)$$

The prediction error is relatively small based on the existing prediction model. Hence, the number of missing tiles is smaller than the number of tiles hit by prediction. Based on the visual perception and

joint consideration between $\chi(N_p, Z_0)$ and $\chi(N_m, Z_1)$, we set

$$\eta_m \leq \eta_p. \quad (3)$$

The QoE in [26] is formulated by the weighted average of video quality minus the weighted spatial video quality. Generally, the distortion of each tile depends on the encoding rate while the spatial video quality can be determined by $N_m \cdot (\eta_p - \eta_m)$. As the number of hit tiles is greater than that of missing tiles, the encoding rate of predictive tiles is the quality of major tiles, which is near the average video quality. Thus, the average mean squared error and the spatial quality variance can be controlled by η_p and $N_m \cdot (\eta_p - \eta_m)$ jointly through weight adjustment. A QoE score is intuitively formulated as the encoding rate of predictive tiles subtracting the perceptual difference, a penalty factor. Based on Assumption 1, we can assess QoE in a video frame within T_1 . Hence, the optimization objective is formulated as

$$\begin{aligned} (\mathbf{P0}) \quad & \max_{\eta_p, \eta_m} \quad \frac{1}{K} \sum_{k=1}^K \alpha_k \eta_p - \beta_k N_m \cdot (\eta_p - \eta_m) \\ \text{s.t.} \quad & (1), (2), (3) \\ & \eta_m, \eta_p \in \{R_1, \dots, R_d, \dots, R_D\} \end{aligned} \quad (4)$$

where for user k , we assign weights α_k and β_k for the encoding rate of predictive tiles and the encoding rate difference $(\eta_p - \eta_m)$, respectively. Particularly, based on human visual system and saliency influence in [10], [34], larger saliency degree in VR FoV carries out larger visual impact, especially in the case of perceptual difference. Thus, α_k and β_k are positively related to saliency degree, especially for β_k .

Problem analysis: In the multi-user massive MIMO systems, variables N_p , N_m , and transmission mode jointly determine $\chi(N_p, Z_0)$, $\chi(N_m, Z_1)$, and $\chi(N_m, Z_2)$, which further decide the average QoE score. The existing basic transmission mode, e.g., uni-stream multicast in [20], which counts indices of tiles for all active users and transmits each tile by uni-stream multicast, is unable to meet the needs of VR 360° video transmission. Thus, optimizing the transmission mode for VR 360° video in massive MIMO systems is necessary. Normally, optimized transmission mode in massive MIMO systems is related to the tile grouping method of multiple tiles, which aims to maximize the overall network throughput.

Under a certain transmission mode, integer η_m in constraint (1) is linear with integer N_m , whereas integers η_p and η_m in constraint (2) are linear with respect to integers N_p and N_m . Furthermore, $N_m(\eta_p - \eta_m)$ is a product of integers N_m and $\eta_p - \eta_m$. Hence, the problem **(P0)** is a high complexity INLP problem. Solving this INLP problem directly would be impractical for real-time transmission. Hence, we consider low complexity alternatives by jointly considering transmission mode, variables N_p and N_m .

To solve problem **(P0)** efficiently and approximately, we first derive the achievable spectral efficiency to establish a basic foundation to optimize tile grouping. We then examine the relationship between N_p and N_m , as well as the product $N_m(\eta_p - \eta_m)$ to efficiently optimize the QoE.

III. ACHIEVABLE SPECTRAL EFFICIENCIES IN TILE TRANSMISSION

In this section, we analyze the SE of VR video by the major linear MRT and ZF precoding in massive MIMO systems. In massive MIMO systems, the tile transmission is either unicast or multicast, and the transmitted data are either uni-stream or multi-stream. We focus on the multi-stream multicast in the VR video transmission process. We index the multiple groups formed by all transmitted tiles of each frame by the index set $\mathcal{G} = \{1, \dots, g, \dots, G\}$, and the multiple streams in each group queue for transmission. We indicate the indices of users requesting tile in group g by a signal matrix \mathbb{J}_g with F rows and B columns, where the (f, b) -th entry $\mathbb{J}_g(f, b)$ represents the index of the b -th user that requests the f -th tile stream in group g . We further use $\mathfrak{J}_{g,f}$, $f = 1, \dots, F$, to represent the set of users in the f -th row of \mathbb{J}_g .

A. Channel Estimation

We define a pilot matrix $\Phi_g = \sqrt{\sigma_g} [\phi_{g,1}, \dots, \phi_{g,f}, \dots, \phi_{g,F}]$, composed by σ_g mutually orthogonal σ_g -length pilot sequences, where $\phi_{g,f}$ is a pilot sequence for each user in $\mathfrak{J}_{g,f}$. The received uplink signal at the BS is

$$\mathbf{Y}_g = \mathbf{H}_g \Phi_g + \mathbf{N}_g \quad (5)$$

where matrix \mathbf{H}_g is formed by entries $\mathbf{H}_g(f, b)$. Each entry $\mathbf{H}_g(f, b)$ represents the channel response of user $\mathbb{J}_g(f, b)$, and $\mathbf{N}_g \in \mathbb{C}^{N \times \sigma_g}$ is the normalized additive noise matrix with entries $\mathbf{N}_g(t, s) \sim \mathcal{CN}(0, 1)$. Thus, we have

$$\mathbf{Y}_g = \sum_{i=1}^F \sum_{b=1}^B \sqrt{\sigma_g q^u} \mathbf{H}_g(i, b) \phi_{g,i}^T + \mathbf{N}_g \quad (6)$$

where q^u is the normalized uplink power. We can obtain the received sequence from \mathbf{Y}_g via

$$\mathbf{y}_{g,f} = \mathbf{Y}_g \phi_{g,f}^* = \sum_{b=1}^B \sqrt{\sigma_g q^u} \mathbf{H}_g(f, b) + \mathbf{n}_{g,f} \quad (7)$$

where $\mathbf{n}_{g,f} \sim \mathcal{CN}(\mathbf{0}, \mathbf{I}_N)$ is normalized additive noise vector corresponding to the users in $\mathfrak{J}_{g,f}$. According to the MMSE estimation proposed in [37], BS can estimate the channel response $\mathbf{H}_g(f, b)$ as follows

$$\tilde{\mathbf{H}}_g(f, b) = \frac{\sqrt{\sigma_g q^u} \Psi_g(f, b)}{1 + \sum_{t=1}^B \sigma_g q^u \Psi_g(f, t)} \left(\sum_{t=1}^B \sqrt{\sigma_g q^u} \Psi_g(f, b) \mathbf{H}_g(f, t) + \mathbf{n}_{g,f} \right) \quad (8)$$

where $\Psi_g(f, b)$ is the large-scale fading coefficient of $\mathbb{J}_g(f, b)$, and $\tilde{\mathbf{H}}_g(f, b) \sim \mathcal{CN}(\mathbf{0}, \mathbf{U}_g(f, b)\mathbf{I}_N)$ with $\mathbf{U}_g(f, b) = \frac{\sigma_g q^u (\Psi_g(f, b))^2}{1 + \sum_{t=1}^B \sigma_g q^u \Psi_g(f, t)}$. Due to the linear combination, we estimate $\mathbf{h}_{g,f}$, the channel response for $\mathbb{J}_{g,f}$, to be $\sum_{t=1}^B \sqrt{\sigma_g q^u} \mathbf{H}_g(f, t)$ and we have

$$\tilde{\mathbf{h}}_{g,f} = \frac{\sum_{t=1}^B \sigma_g q^u \Psi_g(f, t)}{1 + \sum_{t=1}^B \sigma_g q^u \Psi_g(f, t)} \left(\sum_{t=1}^B \sqrt{\sigma_g q^u} \Psi_g(f, t) \mathbf{H}_g(f, t) + \mathbf{n}_{g,f} \right) \quad (9)$$

where $\tilde{\mathbf{h}}_{g,f} \sim \mathcal{CN}(\mathbf{0}, \mu_{g,f} \mathbf{I}_N)$ with $\mu_{g,f} = \frac{(\sum_{t=1}^B \sigma_g q^u \Psi_g(f, t))^2}{1 + \sum_{t=1}^B \sigma_g q^u \Psi_g(f, t)}$. Thus, we have

$$\tilde{\mathbf{H}}_g(f, b) = \frac{\sqrt{\sigma_g q^u} \Psi_g(f, b)}{\sum_{t=1}^B \sigma_g q^u \Psi_g(f, t)} \tilde{\mathbf{h}}_{g,f}. \quad (10)$$

Note that unicast has the same derivation, and the difference is that $\sum_{t=1}^B \sigma_g q^u \Psi_g(f, t)$ in (8)-(10) is equal to $\sigma_g q^u \Psi_g(f, b)$.

B. Achievable Spectral Efficiency in Downlink Transmission

The received sequence of users in group g is

$$\mathbf{r}_g = \mathbf{H}_g^H \mathbf{B}_g \mathbf{s}_g + \mathbf{N}_g \quad (11)$$

where $\mathbf{s}_g = [s_{g,1}, \dots, s_{g,f}, \dots, s_{g,F}]^H$ represents the transmitted sequence of data symbols and $\mathbf{B}_g = [\mathbf{b}_{g,1}, \dots, \mathbf{b}_{g,F}]$ is the precoding matrix of group g in the system. Hence, the received signal of user $\mathbb{J}_g(f, b)$ is

$$\mathbf{r}_g(f, b) = \mathbf{H}_g(f, b)^H \mathbf{B}_g \mathbf{s}_g + \mathbf{N}_g(f, b). \quad (12)$$

1) *MRT Precoding*: The precoding vector for the tile to $\mathbb{J}_{g,f}$ is

$$\mathbf{b}_{g,f}^{\text{MRT}} = \sqrt{\frac{q_{g,f}^d}{N \mu_{g,f}}} \tilde{\mathbf{h}}_{g,f} \quad (13)$$

where $q_{g,f}^d$ is the downlink power of the precoding vector for $\mathbb{J}_{g,f}$. The received signal of user $\mathbb{J}_g(f, b)$ is

$$\mathbf{r}_g^{\text{MRT}}(f, b) = \mathbf{H}_g(f, b)^H \mathbf{b}_{g,f}^{\text{MRT}} s_{g,f} + \sum_{i=1, i \neq f}^F \mathbf{H}_g(f, b)^H \mathbf{b}_{g,i}^{\text{MRT}} s_{g,i} + \mathbf{N}_g(f, b). \quad (14)$$

Hence, the signal-to-interference-plus-noise-ratio (SINR) of user $\mathbb{J}_g(f, b)$ is

$$\Omega_g^{\text{MRT}}(f, b) = \frac{\left| \mathbb{E} \left\{ \mathbf{H}_g(f, b)^H \mathbf{b}_{g,f}^{\text{MRT}} \right\} \right|^2}{1 - \left| \mathbb{E} \left\{ \mathbf{H}_g(f, b)^H \mathbf{b}_{g,f}^{\text{MRT}} \right\} \right|^2 + \sum_{i=1}^F \mathbb{E} \left\{ \left| \mathbf{H}_g(i, b)^H \mathbf{b}_{g,i}^{\text{MRT}} \right|^2 \right\}}. \quad (15)$$

Based on the derivation in [33], $\Omega_g^{\text{MRT}}(f, b)$ is

$$\Omega_g^{\text{MRT}}(f, b) = \frac{Nq_{g,f}^d \mathbf{U}_g(f, b)}{1 + \Psi_g(f, b)P} \quad (16)$$

where P is the total normalized downlink power. And the corresponding SE is

$$\Gamma_g^{\text{MRT}}(f, b) = (1 - \frac{\sigma_g}{T}) \log_2(1 + \Omega_g^{\text{MRT}}(f, b)). \quad (17)$$

2) *ZF Precoding*: The precoding vector for tile g_f is

$$\mathbf{b}_{g,f}^{\text{ZF}} = \sqrt{(N - \sigma_g)q_{g,f}^d \mu_{g,f}} \tilde{\mathbf{H}}_g \left(\tilde{\mathbf{H}}_g^H \tilde{\mathbf{H}}_g \right)^{-1} \mathbf{e}_{g,f} \quad (18)$$

where $\mathbf{e}_{g,f}$ is the f -th column of a identity matrix \mathbf{I}_{σ_g} . The received signal is

$$\mathbf{r}_g^{\text{ZF}} = \sum_{i=1}^F s_{g,i} \mathbf{H}_g^H \mathbf{b}_{g,i}^{\text{ZF}} + \mathbf{N}_g. \quad (19)$$

By replacing \mathbf{H}_g^H with $\mathbf{Z} \tilde{\mathbf{H}}_g^H - \hat{\mathbf{H}}_g^H$, where $\hat{\mathbf{H}}_g$ and \mathbf{Z} are the estimation error $\mathbf{H}_g - \tilde{\mathbf{H}}_g$ and a diagonal matrix $\left[\frac{\sqrt{\sigma_g q^u \Psi_g(1,1)}}{\sum_{i=1}^B \sigma_g q^u \Psi_g(1,i)}, \dots, \frac{\sqrt{\sigma_g q^u \Psi_g(F,B)}}{\sum_{w=1}^B \sigma_g q^u \Psi_g(F,w)} \right]$ based on (10), respectively, \mathbf{r}_g^{ZF} turns to be

$$\mathbf{r}_g^{\text{ZF}} = \sum_{i=1}^F s_{g,i} \left(\mathbf{Z} \tilde{\mathbf{H}}_g^H \mathbf{b}_{g,i}^{\text{ZF}} - \hat{\mathbf{H}}_g^H \mathbf{b}_{g,i}^{\text{ZF}} \right) + \mathbf{N}_g. \quad (20)$$

In (20), matrix $\hat{\mathbf{H}}_g$ is formed by entries $\hat{\mathbf{H}}_g(f, b)$, where entry $\hat{\mathbf{H}}_g(f, b)$ is the estimation error of channel response for $\mathbb{J}_g(f, b)$. $\tilde{\mathbf{H}}_g^H \mathbf{b}_{g,i}^{\text{ZF}}$ is equal to $\sqrt{(N - \sigma_g)q_{g,f}^d \mu_{g,f}} \mathbf{e}_{g,i}$ according to (18); thus, we have

$$\mathbf{r}_g^{\text{ZF}}(f, b) = \frac{\sqrt{(N - \sigma_g)q_{g,f}^d \mu_{g,f} \sigma_g q^u \Psi_g(f, b)}}{\sum_{t=1}^B \sigma_g q^u \Psi_g(f, t)} s_{g,f} - \sum_{i=1}^F \hat{\mathbf{H}}_g(f, b)^H \mathbf{b}_{g,i}^{\text{ZF}} s_{g,i} + \mathbf{N}_g(f, b). \quad (21)$$

Based on the derivation in [33], the SINR of user $\mathbb{J}_g^{\text{ZF}}(f, b)$ is

$$\Omega_g^{\text{ZF}}(f, b) = \frac{(N - \sigma_g) q_{g,f}^d \mathbf{U}_g(f, b)}{1 + P(\Psi_g(f, b) - \mathbf{U}_g(f, b))}. \quad (22)$$

And the corresponding SE is

$$\Gamma_g^{\text{ZF}}(f, b) = (1 - \frac{\sigma_g}{T}) \log_2(1 + \Omega_g^{\text{ZF}}(f, b)). \quad (23)$$

Note that uni-stream transmission has the same derivation, and the difference is that \mathbf{B}_g and \mathbf{s}_g in (11) are a single vector and a one-dimensional data symbol, respectively.

C. Max-Min Fairness

In a multi-stream group, the common performance metric is MMF, where we want to maximize the minimal SINR among the streams. For MRT, the target is $\max_{q_{g,f}^d} \min_{\mathbf{A}_g^{\text{MRT}}(f,b)} \mathbf{A}_g^{\text{MRT}}(f,b) q_{g,f}^d$, where $\mathbf{A}_g^{\text{MRT}}(f,b) = (N\mathbf{U}_g(f,b))/(1 + \Psi_g(f,b)P)$, is the (f,b) -th entry of a power coefficient matrix \mathbf{A}_g . For the user set $\mathcal{I}_{g,f}$, we extract the minimal value in the set $\{\mathbf{A}_g^{\text{MRT}}(f,1), \dots, \mathbf{A}_g^{\text{MRT}}(f,b), \mathbf{A}_g^{\text{MRT}}(f,B)\}$ as the minimal power coefficient $a_{g,f}^{\text{MRT}}$, yielding the solution $q_{g,f}^d = \frac{P}{a_{g,f}^{\text{MRT}}} / \sum_{t=1}^F \frac{1}{a_{g,t}^{\text{MRT}}}$. Likewise, the power coefficient $\mathbf{A}_g^{\text{ZF}}(f,b)$ is $(N - \sigma_g) q_{g,f}^d \mathbf{U}_g(f,b) / [1 + (\Psi_g(f,b) - \mathbf{U}_g(f,b))P]$, and we also extract their minimal value as the minimal power coefficient $a_{g,f}^{\text{ZF}}$, yielding the solution $q_{g,f}^d = \frac{P}{a_{g,f}^{\text{ZF}}} / \sum_{t=1}^F \frac{1}{a_{g,t}^{\text{ZF}}}$.

Hence, the SINRs of each stream in group g by either MRT precoding or ZF precoding are the same, which are denoted as $\Omega_{g,\epsilon}^{\text{MRT}} = \log_2(1 + P / \sum_{t=1}^F \frac{1}{a_{g,t}^{\text{MRT}}})$ and $\Omega_{g,\epsilon}^{\text{ZF}} = \log_2(1 + P / \sum_{t=1}^F \frac{1}{a_{g,t}^{\text{ZF}}})$, respectively. The achievable SEs of each stream in group g are also the same, which are denoted as $\Gamma_{g,\epsilon}^{\text{MRT}} = (1 - \sigma_g/T) \Omega_{g,\epsilon}^{\text{MRT}}$ and $\Gamma_{g,\epsilon}^{\text{ZF}} = (1 - \sigma_g/T) \Omega_{g,\epsilon}^{\text{ZF}}$, respectively. Note that the rule for predictive groups is also applicable to missing groups, and we denote the missing group set as $\mathcal{J} = [1, \dots, j, \dots, J]$.

IV. MULTI-STREAM GROUPING BASED ON VIEWPORT

In this section, we try to search the optimal multi-stream grouping in VR video massive MIMO systems, the SE of which is derived in Section III. According to the equations (17) and (23), we have that decreasing the group number G and the length of pilot sequence σ_g is the key to maximize the systems throughput. We analyze both the characteristics and constraints of multi-streaming group, and proposed a multi-stream grouping method based on multiple viewports. Note that the predictive tiles can be obtained; thus we firstly analyze the predictive tiles.

A. Multi-Stream Group Based on Viewport Tiles

According to the assumption that the number of predictive tiles among users is the same, multiple users may have the same viewport in HMDs simultaneously. Note that the number of different viewports among users relates to the difference of users' favors. We treat these users, who have the same viewport in HMDs, as one entity. The number of entities is equal to the number of different viewports. To make clear the relationship between users and tiles for taking advantage of multicast, we classify the all transmitted tiles of K users into L viewports, and index the viewport set as $\mathcal{L} = \{1, \dots, l, \dots, L\}$ ³. Each viewport has its corresponding viewport tiles and viewport users.

³Turning users into viewport set, we can ignore the specific unicast and multicast.

In a multi-stream group g , we use $\mathbf{p}_g(l, f)$ as an indicator of whether the users of viewport l retrieve the f -th tile stream. Those users with viewpoint l that can retrieve tile f in group g are associated with indicator $\mathbf{p}_g(l, f)=1$; otherwise, $\mathbf{p}_g(l, f)=0$. The users of one viewport can only reliably receive no more than one tile simultaneously; thus, we have

$$0 \leq \mathbf{p}_g(l, f_1) + \mathbf{p}_g(l, f_2) \leq 1, \quad f_1 \neq f_2. \quad (24)$$

Note that there is no restriction among the tiles in one group according to equation (24). Selecting two tiles belonging to viewport l as two streams into group g , those users with viewport l can only receive one of two tiles once and retrieve the other in a new group. It causes an increase in the number of transmitted groups, which leads to the performance degradation. To solve it, each tile stream in a group belongs to a distinct viewport. To search the optimal grouping method, we extend the conception of (24). A tile f in group g that belongs to a viewport l is associated with indicator $\mathbf{d}_g(l, f) = 1$; otherwise, $\mathbf{d}_g(l, f) = 0$. Thus we can write

$$0 \leq \mathbf{d}_g(l, f_1) + \mathbf{d}_g(l, f_2) \leq 1, \quad f_1 \neq f_2. \quad (25)$$

Note that constraint (24) is a basic condition for stable transmission and constraint (25) is a necessary condition for the optimal grouping. Further, selecting more viewports into a group, which slightly increases the length of pilot sequence, can reduce the group number G . Empirically, the influence from the increased length of pilot sequence is relatively smaller than that from the reduced group number⁴. Also, reducing the length of pilot sequence under the minimum group number is necessary.

For a certain tile f , it belongs to one viewport or multiple viewports. To distinguish the two tile types, we define the former as isolated tile (IT), and the latter as coexisting tile (CT). To clarify the relationship between tile and viewport, we analyse a simple viewport set $\mathcal{L} = \{l_1, l_2, l_3\}$. Denote the CTs only belonging to l_1 and l_2 as $\xi(l_1, l_2)$, the CTs of l_3 as $\xi(\sum l_3)$, the ITs of l_3 as $\xi(l_3)$, and the CTs removing l_2 from $(\sum l_3)$ as $\xi(\sum l_3 - l_2)$, respectively. And they follow

$$\begin{cases} \xi(l_1, l_2, l_3) \subseteq \xi(\sum l_3) \\ \xi(l_1, l_3) \subseteq \xi(\sum l_3 - l_2) \\ \xi(l_2, l_3) \subseteq \xi(\sum l_3 - l_1) \end{cases} \quad (26)$$

Further, we denote the number of CTs $\xi(l_1, l_2)$, ITs $\xi(l_3)$, and CTs $\xi(\sum l_3 - l_2)$ as $\Pi(l_1, l_2)$, $\mathcal{A}(l_3)$, and

⁴The worst case is basic grouping method which has the maximum group number and the minimum length of pilot sequence.

$\Pi(\sum l_3 - l_2)$, respectively. Then, we have

$$\Pi(l_1, l_3) + \Pi(l_2, l_3) + \Pi(l_1, l_2, l_3) = N_p - \mathcal{A}(l_3) - \Pi\left(\sum l_3 - l_1 - l_2\right). \quad (27)$$

Based on the distribution of viewport tiles in the HMD scene, we define the viewport that has no IT as coexisting viewport (CV) and that has at least one IT as isolated viewport (IV).

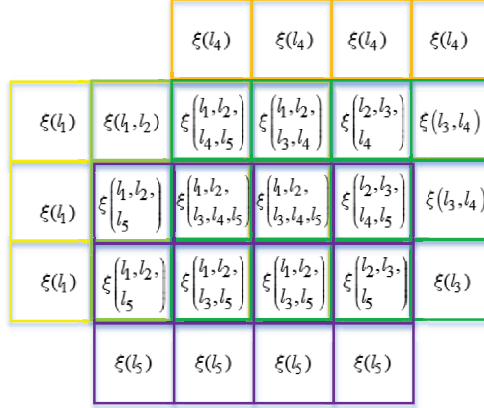


Fig. 5. An example of viewports relation in multi-stream groups.

For clarity, we utilize an example illustrated in Fig. 5 to elaborate the relation of multiple viewports. Each rectangular viewport has 4 tiles in the length and 3 tiles in the width, and we denote its formate as 4×3 . We also draw the relationship among viewports in the tile region and illustrate the relationship of equations (25) and (26) by the graph. After selecting tile $\xi(l_1)$ into multi-stream group g , tile $\xi(l_1, l_2)$ is unable to join in group g . Further, selecting tile $\xi(l_1)$ and tile $\xi(\sum l_3 - l_2)$ into multi-stream group g , each tile of viewport l_2 is unable to join in group g . Normally, CVs always connect with other viewports and are unable to be selected alone, and IVs are the opposite. Note that the goal is to select all viewport tiles into minimal groups under constraint (25). Hence, the focus of tile selection mainly locates on the combination between CVs.

After selecting a viewport tile into a group, the rest viewport tiles form a new graph. And the new selection in another group is processed based on the new graph. The process continues until there is no tile left.

B. Optimal Multi-Stream Grouping Based on Rectangular Viewport

In order to facilitate the following description, we make two definitions as follows:

Definition 1: Combing multiple tiles to form a multi-stream group is defined as combination, and the operation symbol is defined as \cup .

Definition 2: The group containing all viewports is a complete group, denoted as Υ .

The optimal result in each selection process is picking out all viewports in the graph and form a complete group. When selecting a viewport tile into a group, whether the other viewports satisfy constraint (25) is unknown. Moreover, the combination basis for every viewport is unknown, and there is no algorithm to guarantee a complete group in each selection process. To analytically search the optimal complete groups, we firstly propose the following proposition:

Proposition 1: Under constraint (25), combination of rectangular viewports with identical shape $h \times v$ has the minimal complete group number $G_{\text{re}} = h \cdot v$, and the combination of tile $\zeta(x, y)$ satisfies

$$\bigcup_{j=-\lfloor \frac{y}{v} \rfloor}^{\lfloor \frac{V-y}{v} \rfloor} \bigcup_{i=-\lfloor \frac{x}{h} \rfloor}^{\lfloor \frac{H-x}{h} \rfloor} \zeta(x + i \cdot h, y + j \cdot v) \stackrel{\text{def}}{=} \Upsilon \quad (28)$$

where $H = \max \{x\}$ and $V = \max \{y\}$.

Proof: See Appendix A. ■

Remark 1: *Proposition 1* firstly reveals the combination relation among all rectangular viewports in the combination problem. Secondly, *Proposition 1* represents that rectangular viewports with identical shapes have the minimal complete group number. Applying the maximum served users in each group and non-repeated tile stream in all groups is able to make the most of multi-stream ability and minimize the length of pilot sequences in massive MIMO systems. It greatly improves the throughput and reduces delay in VR 360° video transmission. Thirdly, $G_{\text{re}} = h \cdot v$ well reflects the relation between transmitted group size and viewport format size.

C. MLMSG on Non-Rectangular Viewport

In the proposed transmission model, the transmitted viewport contains not only the predictive FoV tiles, but also other tiles in the exact scope. Thus, sometimes the shape of transmitted viewport to each user is non-rectangular. Note that the non-rectangular viewports have no minimum complete group number under constraint (25), even though the shape of each viewport is identical. Based on the *Proposition 1*, we can try to structure a rectangular tile entity, i.e., decomposing the non-rectangular viewport l into rectangular tile lattice λ_l and the other rest tiles δ_l ⁵. Then, $|\lambda_l| + |\delta_l| = N_p$. Note that the larger lattice can achieve smaller total length of pilot sequences for likely increasing the ratio of CTs to all tiles. Thus, the shape of each rectangular tile lattice is the largest shape within all non-rectangular viewports. For rectangular tile lattice λ_l , Section IV-B gives the optimal multi-stream grouping. By iterative decomposition, we can

⁵Compared with λ_l , δ_l is relative small and the combination of δ_l is only subject to the basic constraint (24).

decompose the rest tiles δ_l into multiple types of rectangular tile lattices according to the shape of every δ_l . To meet the tile combination requirement, the quantity of each type of rectangular tile lattices for each viewport is the same. For clarity, we describe the process with an illustration given in Fig. 6.

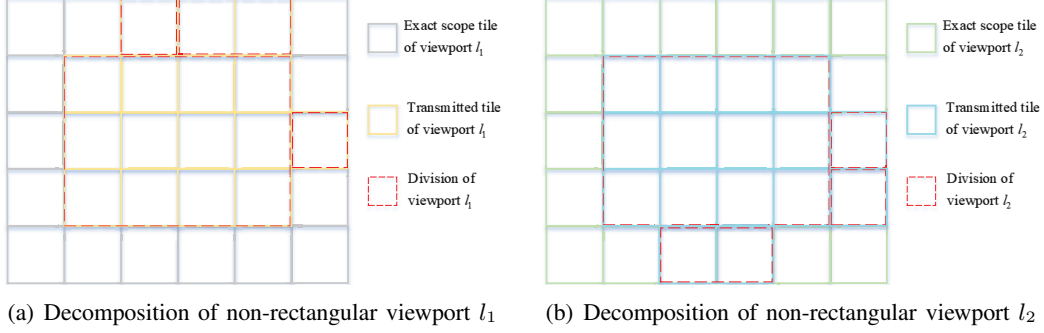


Fig. 6. Decomposition of non-rectangular viewports accordingly to their shapes.

In Fig. 6, the tiles in the red dashed line boxes are tile lattices. The first largest tile lattice is the central 4×3 tile entity. Then, in their rest tiles, there is a lattice including two tiles with identical shapes. Last, the rest one-tile entity forms an one-tile lattice. Hence, we can decompose both non-rectangular viewports l_1 and l_2 into one central 4×3 rectangular tile lattice, one 2×1 rectangular tile lattice, and two 1×1 rectangular tile lattices, respectively.

Note that the combination in each tile lattice set is independent and the equation (28) is still applicable for each type of tile lattice set. Hence, the total group number G_{re} is equal to N_p^6 , and the stream number in each group is determined. The complexity of the combination of the non-rectangular viewports is linear with N_p , namely, $\mathcal{O}(N_p)$. Note that the MLMSG is also suitable for missing viewport tiles, and the complexity is $\mathcal{O}(N_m)$.

V. AVERAGE QoE MAXIMIZATION

The traditional retrieving method only fetches and buffers the predictive FoV tiles, which ignores the missing tiles. The missing tiles do appear in the practical scenario, which causes QoE degradation and even unacceptable VR sickness. In this section, we jointly consider the predictive transmission and the supplementary transmission for missing tiles, and explore the effect of N_p on the average maximum QoE.

Without fully accurate prediction, prediction error occurs and is closely related to exceptional motion [7], which is caused by the multi-stimuli in HMDs. Researchers in [24] leverage realism loss and

⁶When the N_p^k is different for different users, the decomposition method is still applicable, and the group number G_{re} is equal to $\max\{N_p^k\}$.

reconstruction loss to predict the intensity of exception motion of fragment frames, which can provide experimental evidence on the exact scope. Hence, the size of exact scope tiles is a function of the stimuli, which can be obtained based on the previous prediction model. Generally, we assume that the request probability of each tile in the exact scope is equal. Thus, the expected number of missing tiles N_m is

$$N_m = \left\lceil M \cdot \frac{S - N_p}{S} \right\rceil \quad (29)$$

where M and S are the tiles number of FoV format and exact scope format, respectively.

According to the expression of achievable SE and multi-stream grouping,

$$\begin{cases} G = N_p \\ J = N_m. \end{cases} \quad (30)$$

Hence, N_p is also an optimization variable that determines G and J . Thus, we reformulate problem **(P0)** into problem **(P1)**

$$\begin{aligned} \text{(P1)} \quad & \max_{\eta_p, \eta_m, N_p} \quad \frac{1}{K} \sum_{k=1}^K \alpha_k \eta_p - \beta_k N_m (\eta_p - \eta_m) \\ \text{s.t.} \quad & (3), (4), (29), (30) \end{aligned}$$

$$\sum_{g=1}^G \frac{T_1 \eta_p}{v_g} + \sum_{j=1}^J \frac{(T_1 - T_2) \eta_m}{v_j} \leq T_1 \quad (31)$$

$$\sum_{j=1}^J \frac{T_2 \eta_m}{v_j} \leq T_y \quad (32)$$

where v_g and v_j are the transmission rates of predictive group g and missing group j , respectively. Note that $v_g = W \cdot \Gamma_{g,\epsilon}$ is achieved in the predictive transmission but v_j is unavailable without knowing specific tile and user.

To solve the unknown v_j and meet the tolerant latency constraint, v_j is suggested to be a valid value, which is little bit smaller than the actual value. For simplicity, the missing groups reuse the definition of predictive groups, i.e., \mathbb{J}_j , $\mathbb{J}_j(f, b)$, $\mathbb{I}_{j,f}$, $\Psi_j(f, b)$, $\mathbf{U}_j(f, b)$, and $\mathbf{A}_j(f, b)$ have similar meanings to \mathbb{J}_g , $\mathbb{J}_g(f, b)$, $\mathbb{I}_{g,f}$, $\Psi_g(f, b)$, $\mathbf{U}_g(f, b)$, and $\mathbf{A}_g(f, b)$, respectively. The differences are that group indices g turn to be j for missing group j .

In terms of transmission rate in j -th missing group by MRT precoding, the SINR of each stream is

the same and we formulate it as

$$\begin{aligned}\Omega_{j,\epsilon}^{\text{MRT}} &= \frac{P}{\sum_{i=1}^F \frac{1}{\min_{b \in \mathcal{J}_{j,i}} (\mathbf{A}_j^{\text{MRT}}(i,b))}} = \frac{P}{\sum_{i=1}^F \frac{1}{\min_{b \in \mathcal{J}_{j,i}} \left[\frac{N \sigma_j q^u (\Psi_j(i,b))^2}{(1 + \sum_{t=1}^B \sigma_j q^u \Psi_j(i,t)) (1 + \Psi_j(i,b)P)} \right]}} \\ &= \frac{NP}{\sum_{i=1}^F \max_{b \in \mathcal{J}_{j,i}} \left[\frac{(1 + \sum_{t=1}^B \sigma_j q^u \Psi_j(i,t)) (1 + \Psi_j(i,b)P)}{\sigma_j q^u (\Psi_j(i,b))^2} \right]}\end{aligned}\quad (33)$$

where $\frac{1 + \Psi_j(i,b)P}{\sigma_j q^u (\Psi_j(i,b))^2}$ decreases monotonously as $\Psi_j(i,b)$ increases. In the worst case, the minimal large-scale fading coefficient in each stream is the same as the minimal one of the total users. Hence,

$$\Omega_{j,\epsilon}^{\text{MRT}} \geq \frac{NP \cdot \frac{\sigma_j q^u \Psi_{\min}^2}{1 + \Psi_{\min}P}}{\sum_{i=1}^F 1 + \sum_{t=1}^B \sigma_j q^u \Psi_j(i,t)} = NP \cdot \frac{\frac{\sigma_j q^u \Psi_{\min}^2}{1 + \Psi_{\min}P}}{\sigma_j + \sigma_j q^u \Psi_{\text{all}}} = NP \cdot \frac{\frac{q^u \Psi_{\min}^2}{1 + \Psi_{\min}P}}{1 + q^u \Psi_{\text{all}}}\quad (34)$$

where $\Psi_{\text{all}} = \sum_{i=1}^F \sum_{t=1}^B \Psi_j(i,t)$, and Ψ_{\min} is the minimal value of the user large-scale fading coefficients. Denote the right term in (34) as $\Omega_{j,\min}^{\text{MRT}}, j \in \mathcal{J}$, which has no association with the length of pilot sequence and group tile index.

Likewise, we formulate the SINR of j -th group by ZF precoding as

$$\begin{aligned}\Omega_{j,\epsilon}^{\text{ZF}} &= \frac{P}{\sum_{i=1}^F \frac{1}{\min_{b \in \mathcal{J}_{j,i}} (\mathbf{A}_j^{\text{ZF}}(i,b))}} = \frac{P}{\sum_{i=1}^F \frac{1}{\min_{b \in \mathcal{J}_{j,i}} \left[\frac{(N - \sigma_j) \cdot \mathbf{U}_j(i,b)}{1 + (\Psi_j(i,b) - \mathbf{U}_j(i,b))P} \right]}} \\ &= \frac{P}{\sum_{i=1}^F \max_{b \in \mathcal{J}_{j,i}} \left[\frac{1 + (\Psi_j(i,b) - \mathbf{U}_j(i,b))P}{(N - \sigma_j) \cdot \mathbf{U}_j(i,b)} \right]}\end{aligned}\quad (35)$$

where $\frac{1 + \Psi_j(i,b)P}{\mathbf{U}_j(i,b)}$ decreases monotonously as $\Psi_j(i,b)$ increases. The worst case is that the minimal large-scale fading coefficient in each stream is Ψ_{\min} . Similarly,

$$\Omega_{j,\epsilon}^{\text{ZF}} \geq \frac{(N - \sigma_j) q^u \Psi_{\min}^2 P}{1 + q^u \Psi_{\text{all}} + (1 + q^u \Psi_{\text{all}}) \Psi_{\min} P - \sigma_j q^u \Psi_{\min}^2 P}\quad (36)$$

where the right term is denoted as $\Omega_{j,\min}^{\text{ZF}}$. The approximate errors in MRT precoding and ZF precoding are extremely small, which are revealed in Section VI.

We denote the minimum SEs of group j in MRT precoding and ZF precoding by $\Gamma_{j,\min}^{\text{MRT}} = (1 - \sigma_j/T) \log_2 (1 + \Omega_{j,\min}^{\text{MRT}})$ and $\Gamma_{j,\min}^{\text{ZF}} = (1 - \sigma_j/T) \log_2 (1 + \Omega_{j,\min}^{\text{ZF}})$, respectively. Further, $\sigma_j, \forall j \in \mathcal{J}$, is unknown. In the worst case, the tile lattices in the multi-stream grouping are all 1×1 tile lattices; thus σ_j is equal to L in $\Gamma_{j,\min}^{\text{MRT}}$ and $\Gamma_{j,\min}^{\text{ZF}}$. Hence, the results v_j of problem **(P1)** in MRT precoding and ZF precoding approximate to $v_j^{\text{MRT}} = W \cdot \Gamma_{j,\min}^{\text{MRT}}$ and $v_j^{\text{ZF}} = W \cdot \Gamma_{j,\min}^{\text{ZF}}$, respectively. Note that the approximation is also able to be applied to predictive tile groups.

By analysing, η_p and η_m in constraints (31) have linear relationship and are also linear with N_p , and

η_m in (32) is linear with N_m , whereas the product of N_m and $(\eta_p - \eta_m)$ makes the optimization objective nonlinear. To make it linear, the general method is to set N_m or $(\eta_p - \eta_m)$ as a constant. N_p , the set of which is $\{M, \dots, S\}$, decides N_m , the cardinality of which is much smaller than that of $(\eta_p - \eta_m)$. Thus, we set N_p as a constant from M to S , and respectively denote $\eta_p(N_p)$ and $\eta_m(N_p)$ as the encoding rates. The final QoE score of the optimization objective is the maximal value among the calculated results.

Note that the two discrete variables η_p and η_m make each calculation non-convex. Based on the general linear programming method, we relax discrete variables into continuous variables and recover them from the optimization solution. Hence, with fixed N_p , we relax $\eta_p(N_p), \eta_m(N_p) \in [R_1, R_D]$, and problem **(P1)** in the calculation turns to be an ILP problem **(P2)**:

$$\begin{aligned}
 \text{(P2)} \quad & \max_{\eta_p(N_p), \eta_m(N_p)} \quad \frac{1}{K} \sum_{k=1}^K \alpha_k \eta_p(N_p) - \beta_k N_m [\eta_p(N_p) - \eta_m(N_p)] \\
 \text{s.t.} \quad & (3), (29), (30), (31), (32) \\
 & \eta_p(N_p), \eta_m(N_p) \in [R_1, \dots, R_d, \dots, R_D]
 \end{aligned} \tag{37}$$

which can be efficiently solved through the convex optimization toolbox [38]. In the fixed N_p calculation, we obtain the optimization solutions $\eta_p(N_p, 1)$ and $\eta_m(N_p, 1)$, which locate in intervals $[R_{d_{N_p}}^1, R_{d_{N_p}+1}^1]$ and $[R_{d_{N_p}}^2, R_{d_{N_p}+1}^2]$, respectively. According to the two-dimensional linear programming, the closest two-dimensional integer point is only relevant to $\eta_p(N_p, 1)$, which is illustrated in Fig. 7 for clarity. Thus, the two variables recovery starts from variable $\eta_p(N_p, 1)$, which is either $R_{d_{N_p}}^1$ or $R_{d_{N_p}+1}^1$. For

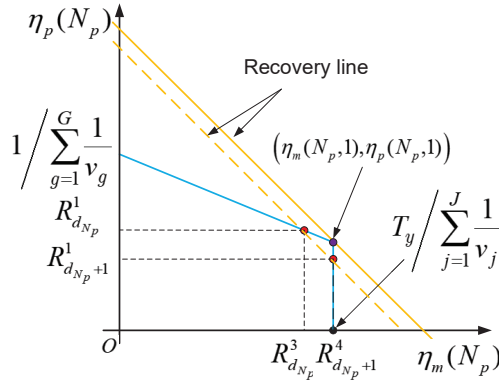


Fig. 7. The recovery policy of two-dimensional integer point.

fixed $R_{d_{N_p}}^1$ and $R_{d_{N_p}+1}^1$, we respectively obtain the optimal encoding rates of missing tiles and indicate them by $R_{d_{N_p}}^3$ and $R_{d_{N_p}+1}^4$, and we use $\mathcal{Q}(N_p, R_{d_{N_p}}^1, R_{d_{N_p}}^3)$ and $\mathcal{Q}(N_p, R_{d_{N_p}+1}^1, R_{d_{N_p}+1}^4)$ to indicate their QoE scores, respectively. Hence, we easily obtain the recovery policy and QoE score in the fixed N_p

calculation as follows

$$\mathcal{Q}_{N_p} = \max \left\{ \mathcal{Q}(N_p, R_{d_{N_p}}^1, R_{d_{N_p}}^3), \mathcal{Q}(N_p, R_{d_{N_p}+1}^1, R_{d_{N_p}+1}^4) \right\}. \quad (38)$$

Therefore, the optimal QoE is

$$\mathcal{Q}_{\text{op}} = \max \{ \mathcal{Q}_S, \dots, \mathcal{Q}_M \}. \quad (39)$$

Therefore, we accordingly obtain the optimal N_p , η_p , and η_m . In addition, the linear programming makes the complexity as $(S - M)\mathcal{O}(K)$, which is a low value.

VI. SIMULATION RESULTS

In the section, we run simulation in Matlab to verify the performance of MLMSG and the joint consideration between predictive tiles and missing tiles in QoE driven VR 360° video massive MIMO transmission.

A. Simulation Setup

We consider VR transmission in a single cell where the radii r_1 and r_2 are 45 meters and 40 meters, respectively. The number of users K and antennas N are 100 and 128, respectively. We model the large-scale fading coefficient for user k as $\psi_k = c/\tau_k^\kappa$, where τ_k is the distance between user k and the BS, $\kappa = 3.76$ is the pass-loss exponent, and $c = 10^{-3.5}$ is a constant [33]. We set the transmission bandwidth W as 100 MHz at a carrier frequency of 2 GHz. The coherence bandwidth and coherence time are 200 kHz and 1 ms, respectively, which contribute to the coherence interval of 200 symbols. We set the noise power spectral density, HMD power P_u , and total downlink power P_d as $\sigma^2 = -174$ dBm/Hz, 0.1 Watts, and 10 Watts, respectively. Thus, the normalized uplink power and total downlink power are $q^u = P_u/(W \cdot \sigma^2)$ and $P = P_d/(W \cdot \sigma^2)$, respectively.

Given that the prediction accuracy decreases sharply as the interval time T_1 increases, T_1 is usually set at 200 ms for high prediction accuracy [35], [39]. Further, we consider a moderate T_2 to balance transmission time with computing time and rendering time. Thus, we set the time interval of the predictive tiles and the missing tiles to $T_1 = 200$ ms and $T_2 = 90$ ms, respectively. The authors [2] recommend the tolerant latency of VR sickness to be $T_y = 10$ ms. In the simulation, the equirectangular format of VR 360° video by tilling projection is 12×12 , and FoV format is 5×4 . The prediction accuracy is about 90% for $T_1 = 200$ ms [35], and the exact scope is a litter larger than the FoV. Thus, we consider three reasonable exact scope formats: 6×4 , 5×5 , and 6×5 . Further, we define the interval of encoding rate of each tile as 10^5 bps. As for the weights of the major tiles quality and the perceptual difference, we adopt

the concept in [26] and consider a moderate variation. Thus, set $\alpha_k = [1.9, 2.1]$, $\beta_k = [\bar{\beta} - 0.02, \bar{\beta} + 0.02]$, where $\bar{\beta} = \{0.1, 0.2, \dots, 1\}$. For clarity, we summarize our simulation parameters in Table I.

TABLE I
SIMULATION PARAMETERS

Parameter	Value	Parameter	Value
N	128	K	100
T	200	T_1	200 ms
T_2	90 ms	T_y	10 ms
α_k	[1.9, 2.1]	β	$\{0.1, \dots, 1\}$
r_1	40	r_2	45
σ^2	-174 dBm/Hz	c	$10^{-3.5}$
κ	3.76	τ_k	$[r_1, r_2]$
P_u	0.1 W	P_d	10 W
W	100 MHz	Equirectangular format	12×12
FoV format	5×4	Encoding rate interval	10^5 bps

B. Performance Evaluations and Comparisons

In this subsection, we show the performance of the proposed MLMSG and adjustment of value N_p in QoE driven VR 360° video massive MIMO transmission. To the best of our knowledge, there has been no previous work proposing a complete system for VR 360° video massive MIMO transmission. The basic grouping (BG) mode derived from uni-stream multicast in [20], is to count the indices of all users' tiles and transmitting each tile by uni-stream multicast. And the previous works on VR 360° video transmission fix value N_p as the FoV size M . Hence, we evaluate and compare the proposed methods in two parts: MLMSG and BG, with variable N_p (VN) and fixed $N_p = M$ (FN), respectively.

To evaluate the approximate processing of v_j described in Section V, we illustrate the actual value and approximate value versus N_m in Fig. 8. We select the exact scope format to be 6×5 ; thus the expected number of missing tile groups $J = N_m$ can change from 1 to 7. In Fig. 8(a), the approximate SINR is extremely close to the actual SINR, and the approximate error is about 0.2%. The approximate SINR and actual SINR by ZF precoding are little larger than those by MRT precoding, respectively. In Fig. 8(b), the average actual SE increases with N_p . The reason is that some tile lattices contain more CTs such that the total pilot sequences turn smaller. The approximation error between the worst approximate SE and the actual SE in missing groups is small and the largest approximation error is 3.5%, which is feasible for performance guarantee.

To evaluate and compare MLMSG and BG, we leverage the transmission delay caused by transmitting one bit of each tile on unit bandwidth, and denote it as ρ , which is unrelated to the encoding

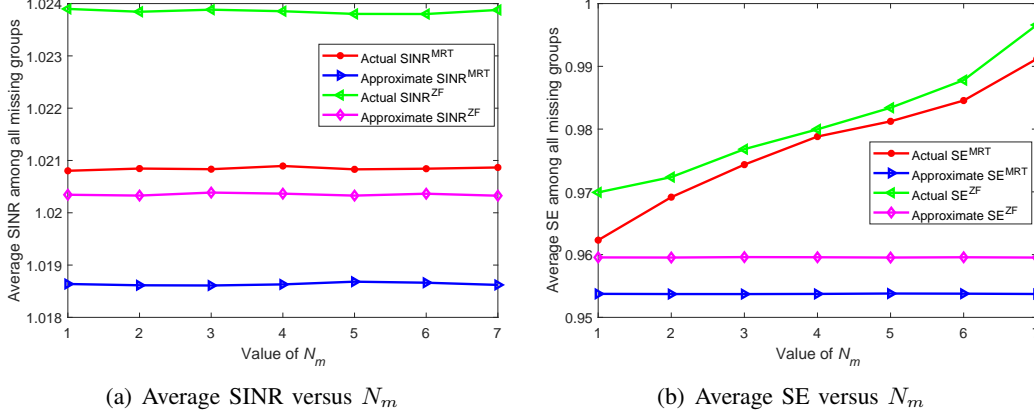


Fig. 8. The comparison between approximate value and actual value.

rate. By MLMSG method, we obtain the approximate value of v_j in advance. But the unknown value $\sum_{t=1}^B \sigma_j q^u \Psi_j(f, t)$ and the variable value J make value v_j in BG method fluctuates over a wide range, which makes it hard to estimate the approximate value of v_j . Thus, we mainly calculate the value of predictive tiles, $\rho = \sum_{g=1}^G 1/\Gamma_{g,\epsilon}$, which well reflects the performances of MLMSG and BG. According to the FoV format 5×4 and three considered exact scope formats, we present the results of ρ with predictive tile formats of 5×4 , 6×4 , 5×5 , and 6×5 in Table II. For this scenario, MRT and ZF have similar behaviors. The value ρ of MLMSG is much smaller than that of BG in all four tile formats, and the reduction is about 23 percent. Compared with BG, the difference is that MLMSG makes the most of the multi-stream ability in MIMO systems and the tile-grouping to reduce group number and length of pilot sequences. It validates that utilizing the multi-stream ability of massive MIMO systems and the optimal multi-stream grouping can greatly improve the throughput and reduce delay in VR 360° video transmission.

TABLE II
EXPERIMENTAL RESULTS (ρ)

Transmission mode	5×4	6×4	5×5	6×5
MLMSG ^{MRT}	19.7507	23.8946	24.5218	29.6776
BG ^{MRT}	26.2308	31.0087	31.7641	37.4574
MLMSG ^{ZF}	19.7411	23.8876	24.5080	29.6666
BG ^{ZF}	26.1884	30.985	31.7241	37.4193

To analyze the performance of average QoE score, we mainly evaluate and compare the combination of MLMSG and VN (MLMSG+VN), the combination of MLMSG and FN (MLMSG+FN), and the combination of BG and FN (BG+FN). Fig. 9 presents the average QoE scores of MLMSG+VN,

MLMSG+FN, and BG+FN. The horizontal axis is the value of $\bar{\beta}$ and the vertical axis is the average QoE score. We restate that higher saliency of multiple stimuli leads to higher $\bar{\beta}$ for user experience. Normally, the average QoE scores of all three methods descend as $\bar{\beta}$ increases. Benefiting from the high throughput, MLMSG can significantly improve the QoE score compared with BG. And MLMSG+VN has a better performance than MLMSG+FN when $\bar{\beta}$ turns larger. For VN, BS adjusts the encoding rate of predictive tiles to reduce the value of penalty factor while the major tiles quality descends. For FN, the penalty factor increases rapidly without adjustment, which leads to the rapid descent of the final QoE score. When the exact scope turns larger, the QoE scores of three algorithms turn smaller for more transmitted tiles and lower encoding rate. Further, the results shows that the difference between MLMSG+VN and MLMSG+FN in Fig. 9(a) and Fig. 9(b) is detectable, though difference between 24 and 25 is little small. It demonstrates that width and height have a little influence on QoE performance. Also, the value of $\bar{\beta}$, which distinguishes MLMSG+VN and MLMSG+FN, turns smaller for the larger exact scope format. For the exact scope with format 6×5 and moderate $\bar{\beta}$, which are closer to the real multi-stimuli VR video, the average QoE score of MLMSG+VN maintains an acceptable level but that of MLMSG+FN decreases sharply as $\bar{\beta}$ increases. It validates that VN aimed at real supplementary transmission of missing tiles can improve and guarantee the QoE score.

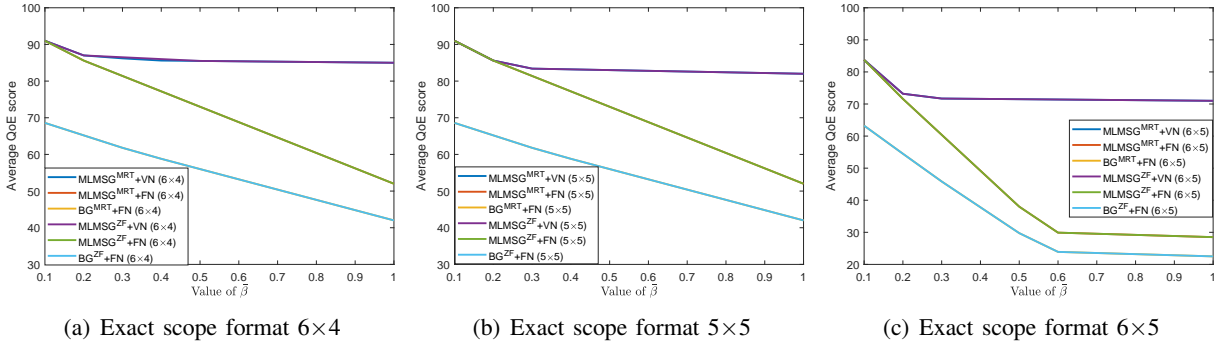


Fig. 9. Average QoE score versus value of $\bar{\beta}$ for different algorithms in three different exact scope formats.

VII. CONCLUSIONS AND FUTURE WORK

In this paper, we have investigated the problem of maximizing the average QoE in VR 360° video massive MIMO transmission. Based on the investigations of the previous works, we considered a practical scenario, and proposed a stable transmission scheme according to the supplementary transmission for missing tiles and unacceptable VR sickness. The integer variables and their relation make the average QoE objective be formulated as an INLP problem. Leveraging the derived expression of the achievable SE of each tile group, we proposed the MLMSG+VN algorithm, and turned the INLP problem into an

ILP problem by fixing the quantity of predictive tiles. With variables relaxation and recovery, we finally achieve the optimal average QoE. Simulation results suggest that our proposed MLMSG+VN algorithm, with pretty low complexity, improves and guarantees VR 360° video QoE. Further, the large improvement validates that the massive MIMO systems with the characteristics of the high overall throughput and the multi-stream ability are very suitable for VR 360° video transmission.

In addition, 360° VR motion sickness, a sensory mismatch between the vestibular system and the visual system, is another challenging issue. The desired scene in the FoV and interactive virtual world should be presented immediately and satisfactorily during user motion, which demands high-rate network links. Given the low latency and high transmission rate of massive MIMO, adapting our method to head motion to improve user experience is an important future direction.

APPENDIX A

PROOF OF PROPOSITION 1

To prove *Proposition 1*, we start with two canonical cases of connection among three $h(h = 4) \times v(v = 3)$ viewports. One case is the maximum viewport connection (MVC) in the horizontal direction as illustrated in Fig. 10(a), and another is the MVC in the vertical direction as shown in Fig. 10(b).

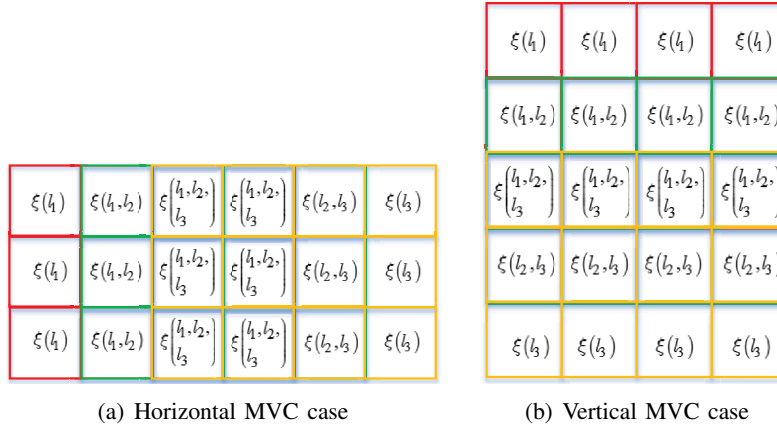


Fig. 10. Two basic cases of three 4×3 viewports.

In both cases, viewport l_2 is CV while viewports l_1 and l_3 are IVs. The number of ITs of viewport l_3 is

$$\mathcal{A}(l_3) = h \cdot v - \Pi(l_2, l_3) - \Pi(l_1, l_2, l_3) \quad (40)$$

where

$$\Pi(l_2, l_3) = h \cdot v - \mathcal{A}(l_2) - \Pi(l_1, l_2) - \Pi(l_1, l_2, l_3). \quad (41)$$

Then, we have

$$\Pi(l_1, l_2) = \mathcal{A}(l_3). \quad (42)$$

With the same derivation, we have

$$\Pi(l_2, l_3) = \mathcal{A}(l_1). \quad (43)$$

Hence, there are enough tiles $\xi(l_3)$ and $\xi(l_1)$ to respectively combine with all CTs $\xi(l_1, l_2)$ and all CTs $\xi(l_2, l_3)$ to form complete groups. In the three-viewport basic cases, we can easily determine the combination relation to form complete group. Further, the combination of tiles indices is related to the size of h and v . Analytically, in the three-viewport horizontal MVC case, for an arbitrary tile $\zeta(x, y)$, $x \in \mathcal{H}$, $y \in \mathcal{V}$, there exists either tile $\zeta(x + h, y)$ or tile $\zeta(x - h, y)$, and combination among them can form a complete group in definition, namely,

$$\zeta(x, y) \cup \zeta(x + h, y) \cup \zeta(x - h, y) \stackrel{def}{=} \Upsilon. \quad (44)$$

When $\zeta(x + h, y)$ or $\zeta(x - h, y)$ in (44) is nonexistent, we can ignore the combination with $\zeta(x + h, y)$ or $\zeta(x - h, y)$, which has no effect on the combination equation. Likewise, in the three-viewport vertical MVC case, for an arbitrary tile $\zeta(x, y)$, $x \in \mathcal{H}$, $y \in \mathcal{V}$, there exists either tile $\zeta(x, y + v)$ or tile $\zeta(x, y - v)$, and

$$\zeta(x, y) \cup \zeta(x, y + v) \cup \zeta(x, y - v) \stackrel{def}{=} \Upsilon. \quad (45)$$

The combination of tile indexes in (44) and (45) enables these three-viewport tiles to form complete groups with number $G_{\text{re}} = h \cdot v$.

When viewport l_1 and l_3 have a connection with other viewports (there are more than three viewports in the graph), (42) and (43) respectively expand to

$$\begin{cases} \Pi(l_1, l_2) = \mathcal{A}(l_3) + \Pi(\sum l_3 - l_1 - l_2) \\ \Pi(l_2, l_3) = \mathcal{A}(l_1) + \Pi(\sum l_1 - l_2 - l_3). \end{cases} \quad (46)$$

Note that the combination of tile indices among viewports l_1, l_2 , and l_3 remains unchanged.

We define the rectangular graph, which has both horizontal MVC and vertical MVC, as full MVC

(FMVC) graph. For clarity, we illustrate a 6×5 FMVC graph with 4×3 viewport tiles in Fig. 11. Note that we can divide the FMVC graph into multiple overlapped MVC graphs and vertical MVC

$\xi(l_1)$	$\xi(l_1, l_2)$	$\xi(l_1, l_2, l_3)$	$\xi(l_1, l_2, l_3)$	$\xi(l_2, l_3)$	$\xi(l_3)$
$\xi(l_1, l_4)$	$\xi(l_1, l_2, l_4)$	$\xi(l_1, l_2, l_4, l_5)$	$\xi(l_1, l_2, l_4, l_5, l_6)$	$\xi(l_2, l_3, l_4)$	$\xi(l_3, l_4, l_5)$
$\xi(l_1, l_4, l_7)$	$\xi(l_1, l_2, l_4, l_7)$	$\xi(l_1, l_2, l_4, l_7, l_8)$	$\xi(l_1, l_2, l_3, l_4, l_5, l_6, l_7, l_8, l_9)$	$\xi(l_2, l_3, l_4, l_5, l_6, l_7, l_8, l_9)$	$\xi(l_3, l_4, l_5, l_6, l_7, l_8, l_9)$
$\xi(l_4, l_7)$	$\xi(l_4, l_5, l_7)$	$\xi(l_4, l_5, l_7, l_8)$	$\xi(l_4, l_5, l_6, l_7, l_8, l_9)$	$\xi(l_5, l_6, l_7, l_8, l_9)$	$\xi(l_6, l_7, l_8, l_9)$
$\xi(l_7)$	$\xi(l_7, l_8)$	$\xi(l_7, l_8, l_9)$	$\xi(l_7, l_8, l_9)$	$\xi(l_8, l_9)$	$\xi(l_9)$

Fig. 11. 6×5 FMVC graph with 4×3 viewport tiles, and also the FMVC graph of the example in Fig. 5.

graphs, and the combination characteristics remain unchanged⁷. Based on the unchanged characteristics, the combination approach is suitable for a $H(H > h) \times V(V > v)$ FMVC graph. And the combination of indexes of tile $\zeta(x, y)$ is

$$\bigcup_{j=-\lfloor \frac{y}{v} \rfloor}^{\lfloor \frac{y-v}{v} \rfloor} \bigcup_{i=-\lfloor \frac{x}{h} \rfloor}^{\lfloor \frac{H-x}{h} \rfloor} \zeta(x+i \cdot h, y+j \cdot v). \quad (47)$$

Each combined group is a complete group, and the group number is $G_{re} = h \cdot v$.

Note that any rectangular viewport graph has its FMVC graph according to the minimal and maximal coordinates. Hence, we easily can achieve any multi-rectangular-viewport graph through its FMVC graph, and the approach is only deleting the nonexistent viewport tiles from the FMVC graph. Further, the combination of indices of tiles remains unchanged, which is the same as (47), and the group number is also $G_{re} = h \cdot v$. The only difference is that $H = \max\{x\}$, $V = \max\{y\}$. Thus, *Proposition 1* is proved.

REFERENCES

- [1] M. T. Hossan, M. Z. Chowdhury, M. Shahjalal, and Y. M. Jang, "Human bond communication with head-mounted displays: Scope, challenges, solutions, and applications," *IEEE Commun. Mag.*, vol. 57, no. 2, pp. 26–32, 2019.
- [2] E. Bastug, M. Bennis, M. Medard, and M. Debbah, "Toward interconnected virtual reality: Opportunities, challenges, and enablers," *IEEE Commun. Mag.*, vol. 55, no. 6, pp. 110–117, 2017.
- [3] Z. Chen, Y. Li, and Y. Zhang, "Recent advances in omnidirectional video coding for virtual reality: Projection and evaluation," *Signal Processing*, vol. 146, pp. 66 – 78, 2018.

⁷Non-rectangular viewport does not have the characteristics.

- [4] M. Xu, Y. Song, J. Wang, M. Qiao, L. Huo, and Z. Wang, "Predicting head movement in panoramic video: A deep reinforcement learning approach," *IEEE Trans. Pattern Anal. Mach. Intell.*, vol. 41, no. 11, pp. 2693–2708, 2019.
- [5] Y. Sun, Z. Chen, M. Tao, and H. Liu, "Communications, caching, and computing for mobile virtual reality: Modeling and tradeoff," *IEEE Trans. Commun.*, vol. 67, no. 11, pp. 7573–7586, 2019.
- [6] T. Dang and M. Peng, "Joint radio communication, caching, and computing design for mobile virtual reality delivery in fog radio access networks," *IEEE J. Sel. Areas Commun.*, vol. 37, no. 7, pp. 1594–1607, 2019.
- [7] H. Hu, Z. Xu, X. Zhang, and Z. Guo, "Optimal viewport-adaptive 360-degree video streaming against random head movement," in *Proc. IEEE Int. Conf. Commun. (ICC)*, 2019, pp. 1–6.
- [8] O. Le Meur, P. Le Callet, D. Barba, and D. Thoreau, "A coherent computational approach to model bottom-up visual attention," *IEEE Trans. Pattern Anal. Mach. Intell.*, vol. 28, no. 5, pp. 802–817, 2006.
- [9] W. Sun, X. Min, G. Zhai, K. Gu, H. Duan, and S. Ma, "MC360IQA: A multi-channel CNN for blind 360-degree image quality assessment," *IEEE J. Sel. Topics Signal Process.*, vol. 14, no. 1, pp. 64–77, 2020.
- [10] Y. Zhu, G. Zhai, X. Min, and J. Zhou, "The prediction of saliency map for head and eye movements in 360 degree images," *IEEE Trans. Multimedia*, vol. 22, no. 9, pp. 2331–2344, 2020.
- [11] J. Zou, C. Li, C. Liu, Q. Yang, H. Xiong, and E. Steinbach, "Probabilistic tile visibility-based server-side rate adaptation for adaptive 360-degree video streaming," *IEEE J. Sel. Topics Signal Process.*, vol. 14, no. 1, pp. 161–176, 2020.
- [12] P. Lungaro, R. Sjöberg, A. J. F. Valero, A. Mittal, and K. Tollmar, "Gaze-aware streaming solutions for the next generation of mobile VR experiences," *IEEE Trans. Vis. Comput. Graphics*, vol. 24, no. 4, pp. 1535–1544, 2018.
- [13] G. J. Sullivan, J. Ohm, W. Han, and T. Wiegand, "Overview of the high efficiency video coding (HEVC) standard," *IEEE Trans. Circuits Syst. Video Technol.*, vol. 22, no. 12, pp. 1649–1668, 2012.
- [14] M. Yu, H. Lakshman, and B. Girod, "A framework to evaluate omnidirectional video coding schemes," in *Proc. IEEE Int. Symp. Mixed Augmented Reality*, 2015, pp. 31–36.
- [15] J. Feng, Y. Wu, G. Zhai, N. Liu, and W. Zhang, "An algorithm for transmitting VR video based on adaptive modulation," in *Proc. IEEE/CIC Int. Conf. Commun. China (ICCC)*, 2019, pp. 443–448.
- [16] Z. Liu, S. Ishihara, Y. Cui, Y. Ji, and Y. Tanaka, "JET: Joint source and channel coding for error resilient virtual reality video wireless transmission," *Signal Processing*, vol. 147, pp. 154 – 162, 2018.
- [17] J. Li, R. Feng, Z. Liu, W. Sun, and Q. Li, "Modeling QoE of virtual reality video transmission over wireless networks," in *Proc. IEEE Global Commun. Conf. (GLOBECOM)*, 2018, pp. 1–7.
- [18] K. Long, C. Ye, Y. Cui, and Z. Liu, "Optimal multi-quality multicast for 360 virtual reality video," in *Proc. IEEE Global Commun. Conf. (GLOBECOM)*, 2018, pp. 1–6.
- [19] H. Yang, T. L. Marzetta, and A. Ashikhmin, "Multicast performance of large-scale antenna systems," in *Proc. IEEE 14th Workshop Signal Process. Adv. Wireless Commun. (SPAWC)*, 2013, pp. 604–608.
- [20] C. Guo, Y. Cui, and Z. Liu, "Optimal multicast of tiled 360 VR video," *IEEE Wireless Commun. Letters*, vol. 8, no. 1, pp. 145–148, 2019.
- [21] K. Long, Y. Cui, C. Ye, and Z. Liu, "Optimal wireless streaming of multi-quality 360 VR video by exploiting natural, relative smoothness-enabled and transcoding-enabled multicast opportunities," *IEEE Trans. Multimedia*, pp. 1–1, 2020.
- [22] L. Zhao, Y. Cui, C. Guo, and Z. Liu, "Optimal streaming of 360 VR videos with perfect, imperfect and unknown fov viewing probabilities," in *Proc. IEEE Global Commun. Conf. (GLOBECOM)*, 2020, pp. 1–6.
- [23] Z. Fei, F. Wang, J. Wang, and X. Xie, "QoE evaluation methods for 360-degree VR video transmission," *IEEE J. Sel. Topics Signal Process.*, vol. 14, no. 1, pp. 78–88, 2020.

- [24] H. G. Kim, H. Lim, S. Lee, and Y. M. Ro, "VRSA Net: VR Sickness Assessment Considering Exceptional Motion for 360° VR Video," *IEEE Trans. Image Process.*, vol. 28, no. 4, pp. 1646–1660, 2019.
- [25] T. Zhao, Q. Liu, and C. W. Chen, "QoE in video transmission: A user experience-driven strategy," *IEEE Commun. Surveys Tuts.*, vol. 19, no. 1, pp. 285–302, 2017.
- [26] J. Fu, X. Chen, Z. Zhang, S. Wu, and Z. Chen, "360SRL: A sequential reinforcement learning approach for ABr tile-based 360 video streaming," in *Proc. IEEE International Conference on Multimedia and Expo (ICME)*, 2019, pp. 290–295.
- [27] C. Perfecto, M. S. Elbamby, J. D. Ser, and M. Bennis, "Taming the latency in multi-user VR 360°: A QoE-aware deep learning-aided multicast framework," *IEEE Trans. Commun.*, vol. 68, no. 4, pp. 2491–2508, 2020.
- [28] T. L. Marzetta, "Noncooperative cellular wireless with unlimited numbers of base station antennas," *IEEE Trans. Wireless Commun.*, vol. 9, no. 11, pp. 3590–3600, 2010.
- [29] A. Adhikary, J. Nam, J. Ahn, and G. Caire, "Joint spatial division and multiplexing—the large-scale array regime," *IEEE Trans. Inf. Theory*, vol. 59, no. 10, pp. 6441–6463, 2013.
- [30] C. Sun, X. Gao, S. Jin, M. Matthaiou, Z. Ding, and C. Xiao, "Beam division multiple access transmission for massive MIMO communications," *IEEE Trans. Commun.*, vol. 63, no. 6, pp. 2170–2184, 2015.
- [31] L. Sanguinetti, E. Björnson, and J. Hoydis, "Toward massive MIMO 2.0: Understanding spatial correlation, interference suppression, and pilot contamination," *IEEE Transactions on Communications*, vol. 68, no. 1, pp. 232–257, 2020.
- [32] Y. Polyanskiy, H. V. Poor, and S. Verdú, "Channel coding rate in the finite blocklength regime," *IEEE Trans. Inf. Theory*, vol. 56, no. 5, pp. 2307–2359, 2010.
- [33] M. Sadeghi, E. Björnson, E. G. Larsson, C. Yuen, and T. Marzetta, "Joint unicast and multi-group multicast transmission in massive MIMO systems," *IEEE Trans. Wireless Commun.*, vol. 17, no. 10, pp. 6375–6388, 2018.
- [34] V. Sitzmann, A. Serrano, A. Pavel, M. Agrawala, D. Gutierrez, B. Masia, and G. Wetzstein, "Saliency in VR: How do people explore virtual environments?" *IEEE Trans. Visu. Comput. Graphics*, vol. 24, no. 4, pp. 1633–1642, 2018.
- [35] F. Qian, B. Han, Q. Xiao, and V. Gopalakrishnan, "Flare: Practical viewport-adaptive 360-degree video streaming for mobile devices," in *Proc. ACM Mobicom*, ser. MobiCom '18. New York, NY, USA: Association for Computing Machinery, 2018, p. 99–114.
- [36] Zhou Wang, A. C. Bovik, H. R. Sheikh, and E. P. Simoncelli, "Image quality assessment: from error visibility to structural similarity," *IEEE Trans. Image Process.*, vol. 13, no. 4, pp. 600–612, 2004.
- [37] S. M. Kay, *Fundamentals of statistical signal processing*, ser. Prentice Hall signal processing series. Upper Saddle River, NJ: Prentice Hall PTR, 1993.
- [38] M. Grant and S. Boyd, "CVX: Matlab software for disciplined convex programming, version 2.1," Mar. 2014.
- [39] X. Hou, S. Dey, J. Zhang, and M. Budagavi, "Predictive adaptive streaming to enable mobile 360-degree and VR experiences," *IEEE Trans. Multimedia*, vol. 23, pp. 716–731, 2021.